

Charmed hadron production in the QGSJET-III model: relevance to calculations of the prompt atmospheric neutrino background

Sergey Ostapchenko and Günter Sigl

Universität Hamburg, II Institut für Theoretische Physik, 22761 Hamburg, Germany

August 19, 2025

Abstract

The treatment of charmed hadron production in the framework of the QGSJET-III Monte Carlo generator is developed, including both perturbative and nonperturbative contributions. For the former, a leading order (LO) perturbative formalism is employed. The so-called K -factor designed to take effectively into account higher order corrections, which controls the magnitude of the LO perturbative contribution, is fixed based on a comparison with experimental data on D meson production at the Large Hadron Collider. For the nonperturbative intrinsic charm, a phenomenological Regge-based treatment is developed, with the corresponding normalization being chosen based on measurements of the spectra of Λ_c baryons at large values of Feynman x . The model is applied for a calculation of the prompt atmospheric muon neutrino flux in the 10 – 100 TeV and 1 – 10 PeV energy intervals.

1 Introduction

Secondary charmed hadrons created in hadronic collisions are much less abundant, compared to the ones composed of light (anti)quarks. Nevertheless, an accurate description of charmed hadron production is of importance for astrophysical studies based on detection of high energy neutrino fluxes [1]. This is because the atmospheric neutrino background created by interactions of high energy cosmic rays (CRs) with air is dominated above ~ 1 PeV by the so-called prompt component, i.e., by neutrinos resulting from decays of charmed hadrons produced in such interactions. The suppression of the “con-

ventional” atmospheric neutrino flux resulting from decays of pions and kaons, at PeV energies, is due to the relatively long life time of such particles. Consequently, very high energy pions and kaons have small chances to decay in flight, before interacting with air nuclei. In contrast, short life time of charmed hadrons allows them to decay and to produce thereby an important background for astrophysical neutrino detection in the PeV energy range.

The production of charm (anti)quarks within the perturbative quantum chromodynamics (pQCD) framework is rather well understood [2, 3]. Moreover, experimental measurements of the production spectra of charmed hadrons, in proton-proton collisions, notably, by the LHCb collaboration [4, 5, 6], allowed one to substantially reduce the uncertainties of the corresponding calculations, related to the low x behavior of parton distribution functions (PDFs) of gluons [7, 8, 9, 10] and concerning the choice of the factorization and renormalization scales (e.g., [11]). Much less constrained is the potential contribution of the nonperturbative intrinsic charm (IC) [12, 13], for which only vague upper bounds have been derived (e.g., [14, 15, 16]).

In this work, a treatment of charmed hadron production in the framework of the QGSJET-III Monte Carlo (MC) generator [17, 18] is developed, including both perturbative and nonperturbative contributions. For the former, a leading order (LO) pQCD description is employed. The so-called K -factor designed to take effectively into account higher order corrections, which controls the magnitude of the LO perturbative contribution, is fixed based on a comparison with LHCb data on D meson production in

proton-proton collisions. For the nonperturbative intrinsic charm, a phenomenological Regge-based treatment is developed, with the corresponding normalization being chosen based on measurements of Λ_c^+ baryon production in pp collisions at the Intersecting Storage Rings (ISR) [19]. A possibility to constrain this normalization, using the upper limit on the prompt atmospheric neutrino background, obtained by the IceCube collaboration [20], is discussed.

The outline of the paper is as follows. In Section 2, the treatment of the perturbative charm production is described. Section 3 is devoted to a phenomenological description of the intrinsic charm contribution. Selected numerical results regarding charm production in proton-proton collisions are presented in Section 4, in comparison to experimental measurements of charmed hadron spectra. The relevance of the developed formalism to calculations of the prompt atmospheric neutrino background and the relative importance of the corresponding perturbative and nonperturbative contributions are discussed in Section 5. Finally, the conclusions are given in Section 6.

2 Perturbative contribution to charm production

The QGSJET-III model [17, 18] treats hadronic collisions within the Reggeon Field Theory framework [21, 22], describing multiple rescattering processes between interacting hadrons (nuclei) as Pomeron exchanges. The latter thus provide an effective description for microscopic (generally nonperturbative) parton cascades mediating the collisions. With increasing energy, such cascades enter the perturbative domain of high parton virtualities q^2 . This leads one to the concept of “semihard Pomeron”: treating the perturbative parton evolution at $q^2 > Q_0^2$, Q_0^2 being some cutoff for pQCD being applicable, by means of the Dokschitzer-Gribov-Lipatov-Altarelli-Parisi (DGLAP) formalism [23, 24, 25], while retaining the phenomenological Pomeron description for the nonperturbative (parts of) parton cascades [26, 27, 28]. Further, one treats nonlinear interaction effects corresponding to a rescattering of intermediate partons in such cascades off the projectile or target hadrons (nuclei) or off each other as Pomeron-Pomeron interac-

tions, based on all order resummation of the respective (so-called enhanced) Pomeron diagrams [29, 30, 31]. Considering unitarity cuts of multi-Pomeron graphs describing hadron-proton (hadron-nucleus, nucleus-nucleus) elastic scattering and applying the so-called Abramovskii-Gribov-Kancheli (AGK) cutting rules [32], one is able to derive both the interaction cross sections for collisions of interest and partial probabilities for various “macro-configurations” of such collisions, i.e., for various topologies of cut Pomeron “nets”, where a cut Pomeron represents an elementary production process [30, 31]. In turn, this allows one to employ MC techniques for sampling collision events [33].

Very remarkably, by virtue of the AGK cancellations [32], the outcome of the above-discussed procedure for parton jet production is consistent with the collinear factorization of pQCD [34] in the sense that the (here LO) inclusive jet production cross section, above a chosen Q_0^2 -cutoff, is described by the usual pQCD factorization ansatz¹ [35, 36]:

$$\begin{aligned} \sigma_{ab}^{\text{jet}}(s, Q_0^2) &= K_f \int dx^+ dx^- d\hat{t} \frac{\pi \alpha_s^2(\mu_R^2)}{\hat{s}^2} \\ &\times \sum_{I,J,I',J'} \frac{1}{1 + \delta_{I'J'}} f_{I/a}(x^+, \mu_F^2) f_{J/b}(x^-, \mu_F^2) \\ &\times |M_{IJ \rightarrow I'J'}(\hat{s}, \hat{t})|^2 \Theta(\mu_F^2 - Q_0^2), \quad (1) \end{aligned}$$

where s is the center-of-mass (c.m.) energy squared for hadron-proton (nucleon-nucleon) interaction, \hat{s} and \hat{t} are Mandelstam variables for parton-parton scattering, x^\pm are light cone (LC) momentum fractions of partons I and J , respectively, α_s is the running coupling, $f_{I/a}$ is the PDF of parton I in particle a , $M_{IJ \rightarrow I'J'}$ is the LO matrix element for the Born $IJ \rightarrow I'J'$ scattering, μ_F and μ_R are the factorization and renormalization scales ($\mu_F = \mu_R = p_\perp/2$ is used, with p_\perp being the transverse momentum of partons I' and J' , produced in the hard process), and the factor $K_f = 1.5$ is designed to take effectively into account higher order pQCD corrections. It is noteworthy that in the above-described model treatment, the PDFs $f_{I/a}$ comprise absorptive corrections due to intermediate parton rescattering off their parent hadrons (nuclei) [17, 35].

The fragmentation of final partons into

¹Modulo higher twist corrections [17].

hadrons involves s -channel parton cascades (so-called final state radiation) and a hadronization of strings of color field stretched between those partons or/and constituent partons of the interacting hadrons (nuclei) [17, 18].

While secondary particle production in the QGSJET-III MC generator was restricted to hadrons composed of light (u , d , and s) (anti)quarks, it can be trivially generalized to include perturbative charm production by adding $gg \rightarrow c\bar{c}$ and $q\bar{q} \rightarrow c\bar{c}$ subprocesses to the right-hand-side of Eq. (1), with the corresponding LO matrix elements squared (e.g., [37])

$$|M_{gg \rightarrow c\bar{c}}(\hat{s}, \hat{t})|^2 = \left(\frac{1}{6\tau_1\tau_2} - \frac{3}{8} \right) \times \left(\tau_1^2 + \tau_2^2 + \rho - \frac{\rho^2}{4\tau_1\tau_2} \right), \quad (2)$$

$$|M_{q\bar{q} \rightarrow c\bar{c}}(\hat{s}, \hat{t})|^2 = \frac{4}{9} (\tau_1^2 + \tau_2^2 + \rho/2). \quad (3)$$

Here $\tau_1 = (m_c^2 - \hat{t})/\hat{s}$, $\tau_2 = (\hat{s} + \hat{t} - m_c^2)/\hat{s}$, $\rho = 4m_c^2/\hat{s}$, and m_c is the c -quark mass (we use $m_c = 1.3$ GeV).

At this step, we choose the factorization and renormalization scales for c -quark production as $\mu_F^c = \mu_R^c = 2m_{c,\perp}$, where $m_{c,\perp} = \sqrt{m_c^2 + p_\perp^2}$, i.e., differently compared to the ones for gluon and light quark production. Correspondingly, we use here a different K -factor, $K_f^c = 3$, whose value has been fixed based on a comparison with LHCb data on $D^0 + \bar{D}^0$ production (see Section 4). Generally, in a LO approach, changes of μ_F and μ_R can be more or less absorbed into a suitable redefinition of the K -factor. Additionally, for our choice of μ_F^c and μ_R^c , the treatment of charm production is independent of the technical parameter of the model, the Q_0^2 -cutoff ($Q_0^2 = 2$ GeV² is used).

Regarding hadron production, including charmed secondaries requires only minor changes in the corresponding MC procedure. After determining the “macro-configuration” of a collision, we proceed as usual with energy-momentum sharing between elementary production processes and with a simulation of t -channel parton cascades (so-called initial state radiation) for semihard scattering processes, using a forward evolution algorithm [17]. Restricting ourselves with three active flavours, the only change is the possibility to produce a $c\bar{c}$ -pair in the hardest scattering process. In

the three flavour evolution scheme employed, produced charm (anti)quarks do not undergo final state cascading. The procedure completes with fragmentation of strings of color field stretched between final partons.

The string fragmentation is modeled as an iterative emission of secondary hadrons from string ends, with the LC momentum fraction x of a hadron (LC⁺ for the projectile side end and LC⁻ for the target side end), being sampled according to the distribution

$$f_{qq' \rightarrow h}(x) \propto x^{1-\alpha_q-\alpha_{q'}} (1-x)^{\Lambda-\alpha_{q'}}, \quad (4)$$

where q is the string end parton, q' is the parton created from the vacuum to form hadron h , and the parameters α_q are expressed via intercepts of the relevant Regge trajectories [18]. For charm (anti)quark as the string end, $\alpha_q = \alpha_c = \alpha_\psi(0) \simeq -2$ [38] and we consider the production of Λ_c (anti)baryons ($\alpha_{q'} = \alpha_{ud} = 2\alpha_N(0) - \alpha_\mathbb{R}$) and D -mesons ($\alpha_{q'} = \alpha_u = \alpha_d = \alpha_\mathbb{R}$), with $\alpha_N(0) = 0$ and $\alpha_\mathbb{R} = 0.5$ [39, 40]. Contributions of the production and decays of heavier charmed hadrons are assumed to be effectively taken into account in the Λ_c (anti)baryon and D meson yields, via the duality principle.

3 Treatment of nonperturbative intrinsic charm

In addition to the perturbative mechanism for charm production, discussed in Section 2, an important contribution to spectra of secondary charmed hadrons may be related to the intrinsic charm content of hadrons [12, 13]. In that regard, it is important to keep in mind that IC (anti)quarks are present in hadrons in a virtual state, being a part of multiparton fluctuations, constituent parton Fock states, “prepared” well in advance of a hadron-proton (hadron-nucleus, nucleus-nucleus) collision [12]. It is therefore the interaction process which can “awake” the intrinsic charm, putting the c and \bar{c} on shell. In our treatment, we follow the approach of [41, 42], assuming that an inelastic interaction of *any* parton constituent of incident hadron is sufficient to destroy the coherence of the initial parton fluctuation and, in case that fluctuation contains a $c\bar{c}$ state, “to free the intrinsic charm from its virtual state” [42]. Thus, the IC content of a

hadron can be characterized by a single parameter, namely, by the relative weight of constituent Fock states containing such $c\bar{c}$ pairs [43]. In our approach, this is slightly modified since we consider a Good-Walker (GW) decomposition of hadron wave functions [44], with different GW states being characterized by different spatial sizes and different (integrated) parton densities [17]. It is natural to expect that in more compact Fock states, the characteristic virtuality of constituent partons is higher, $q_{\text{const}}^2 \propto 1/R_{h(i)}^2$, $R_{h(i)}$ being the transverse size of state $|i\rangle$ of hadron h [45]. Therefore, we assume that a compact $c\bar{c}$ pair is more likely to emerge in a smaller size state, defining the probability for IC to be present in state $|i\rangle$ of hadron h as

$$w_{h(i)}^{\text{IC}} = w_0^{\text{IC}} R_{p(1)}^2 / R_{h(i)}^2, \quad (5)$$

where $R_{p(1)}$ is the size of the largest GW state considered of the proton and w_0^{IC} is the IC content of that state. Based on a comparison with ISR data on Λ_c^+ baryon production, we choose $w_0^{\text{IC}} = 3 \cdot 10^{-4}$ (see Section 4). It is noteworthy that, since the relative role of small size GW states increases with energy [17], the above-discussed assumptions may lead to a slightly faster energy rise of the IC contribution to charmed hadron production, compared to the energy dependence of the inelastic cross section for a reaction.

Regarding the LC momentum fractions x possessed by IC (anti)quarks, we rely on a Regge-based approach: assuming that the corresponding distribution follows the Regge asymptotic, $\propto x^{-\alpha_\psi(0)}$, in the low x limit [38]. As demonstrated in [43], the corresponding momentum distribution is not too different from the one of the original Brodsky-Hoyer-Peterson-Sakai model [12, 13].

The next crucial point concerns the hadronization procedure for IC (anti)quarks. For an incident proton, we assume that the c quark is combined with the valence ud diquark, forming a Λ_c^+ baryon, which is supported by measurements of Λ_c^+ spectra at large values of Feynman x [19, 46, 47]. On the other hand, the remaining valence quark and the \bar{c} are positioned at the ends of strings of color field, resulting from the inelastic scattering process. For incident pions and kaons, we assume a formation of a D meson by the \bar{c} (c) quark and a light valence (anti)quark, while the remaining

valence antiquark (quark) and the c (\bar{c}) work as string ends. Thus, for hadron h with active intrinsic charm, undergoing n inelastic rescatterings, the LC momentum partition between $2n$ string end partons and the “leading” charmed hadron h_c is described by the distribution

$$f_h^{\text{LC}}(x_1, \dots, x_{2n}, x_{h_c}) \propto \left[\prod_{i=1}^{2n-2} x_i^{-\alpha_{\text{sea}}} \right] \times x_{2n-1}^{-\alpha_{q_v}} x_{2n}^{-\alpha_\psi(0)} x_{h_c}^{-\alpha_{h_c}} \delta \left(1 - x_{h_c} - \sum_{j=1}^{2n} x_j \right). \quad (6)$$

Here the exponent α_{sea} is used for sea (anti)quarks while the light valence (anti)quark and the IC c (\bar{c}) follow the Regge behavior: $\propto x_{2n-1}^{-\alpha_{q_v}}$ ($\alpha_u = \alpha_d = \alpha_{\mathbb{R}}$, $\alpha_s = \alpha_\phi(0) = 0$) and $\propto x_{2n}^{-\alpha_\psi(0)}$, respectively. For $h = p$, $h_c = \Lambda_c^+$ and

$$\alpha_{\Lambda_c} = \alpha_{ud} + \alpha_\psi(0) - 1 = 2\alpha_N(0) - \alpha_{\mathbb{R}} + \alpha_\psi(0) - 1, \quad (7)$$

while for h being a pion or kaon, a leading D meson is produced, with $\alpha_D = \alpha_{\mathbb{R}} + \alpha_\psi(0) - 1$. The fragmentation of all final strings, including ones with c or \bar{c} at their ends, is treated as described in Section 2. The parameters involved have been specified above or listed in [18].

4 Selected numerical results for charm production

In Fig. 1, we plot the energy dependence of the cross section for $c\bar{c}$ pair production in proton-proton collisions, $\sigma_{pp}^{c\bar{c}}$, calculated using the above-described formalism, showing also partial contributions of the perturbative and nonperturbative mechanisms². It is easy to see that the latter depends rather weakly on energy, dominating the charm production at relatively low energies only, while constituting a small fraction of $\sigma_{pp}^{c\bar{c}}$ in the very high energy limit. This is not surprising since the intrinsic charm is a property of a hadron wave function, hence, the cross section for IC activation constitutes an approximately constant fraction of the total inelastic cross section for a reaction (see, e.g., the corresponding discussion in [43]). For comparison, we

²IC contributions both from the projectile and target protons are accounted for.

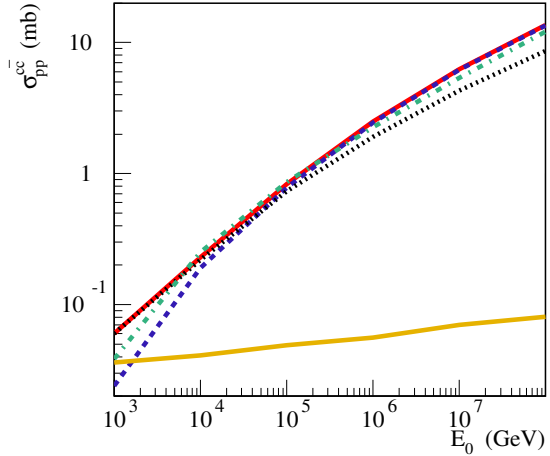


Figure 1: Laboratory energy dependence of the cross section for charm production in pp collisions, $\sigma_{pp}^{c\bar{c}}$, calculated using the default model settings (red solid line); partial contributions of the perturbative and nonperturbative mechanisms to $\sigma_{pp}^{c\bar{c}}$ are shown by blue dashed and yellow solid lines, respectively. $\sigma_{pp}^{c\bar{c}}$ calculated using $\mu_F^c = \mu_R^c = 1.2m_{c,\perp}$ and $K_f^c = 2$ in the pQCD treatment is plotted by black dotted line while the results of Ref. [48] are shown by green dash-dotted line.

also plot in Fig. 1 $\sigma_{pp}^{c\bar{c}}$ calculated in [48], using a next-to-leading order (NLO) DGLAP formalism, with the factorization and renormalization scales, $\mu_F^c = 2.1m_{c,\perp}$ and $\mu_R^c = 1.6m_{c,\perp}$, being adjusted to fit LHCb data on charmed hadron production [11]. At sufficiently high energies, our results for the perturbative contribution to $\sigma_{pp}^{c\bar{c}}$, shown by the dashed line in the Figure, are very close to the ones of Ref. [48], which illustrates the importance of those LHCb measurements for constraining both LO and NLO pQCD predictions.

It is worth repeating that for our LO treatment, we have a certain degeneracy between the choice of the K -factor, K_f^c , and of the factorization and renormalization scales, μ_F^c and μ_R^c , such that changes of the latter two can be more or less absorbed into a suitable redefinition of the former. This is illustrated in Fig. 1, where we plot by the dotted line the charm production cross section obtained using $\mu_F^c = \mu_R^c = 1.2m_{c,\perp}$ and $K_f^c = 2$ for the perturbative contribution. In such a case, however, we have a somewhat slower energy rise of $\sigma_{pp}^{c\bar{c}}$: since for a lower μ_F^c ,

the gluon PDF is probed at a lower virtuality scale, where it is characterized by a less steep low x rise.

Regarding a comparison with accelerator data, we start in Fig. 2 with confronting our calculations of transverse momentum spectra, for a number of rapidity intervals, of $D^0 + \bar{D}^0$ mesons produced in pp collisions at $\sqrt{s} = 5, 7$, and 13 TeV to LHCb measurements³ [4, 5, 6]. While we have an acceptable overall agreement with the data, the calculated cross sections fall down somewhat faster with increasing p_\perp , than observed by the experiment. We also plot as dotted histograms in Fig. 2 the results of our calculations using $\mu_F^c = \mu_R^c = 1.2m_{c,\perp}$ and $K_f^c = 2$ in the pQCD treatment. Clearly, they are rather similar to our default case, except that the slower energy rise of the perturbative charm production for these settings improves somewhat the agreement with the data at $\sqrt{s} = 7$ TeV, while leading at the same time to a sizable underestimation of the $D^0 + \bar{D}^0$ yield at $\sqrt{s} = 13$ TeV.

Concerning the intrinsic charm, its contribution to the results plotted in Fig. 2, shown by the dash-dotted lines in the Figure, proves to be miserable. Therefore, the IC content of the proton can not be reliably constrained by those LHCb data. In that regard, our main experimental constraint comes from measurements of Λ_c^+ baryon production at large values of Feynman x in pp collisions at ISR [19]. Our calculations are compared to the data on Feynman x distribution of Λ_c^+ in Fig. 3. Clearly, the calculated Λ_c^+ yield comes predominantly from the intrinsic charm, with the perturbative contribution shown by the dashed line in the Figure, being negligibly small in the kinematic range studied. While the error bars for the experimental data are rather large, an additional constraint on the IC content is provided by measurements of D meson production in pp collisions at 800 GeV/c by the LEBC-MPS collaboration [49], our calculations being compared to the data in Fig. 4. Here it is easy to see that our normalization for the IC content of the proton likely corresponds to the upper bound: the calculated x_F dependence of D meson yield is systematically flatter than the observed one.

³The measured $D^0 + \bar{D}^0$ yields comprise contributions of D^* decays.

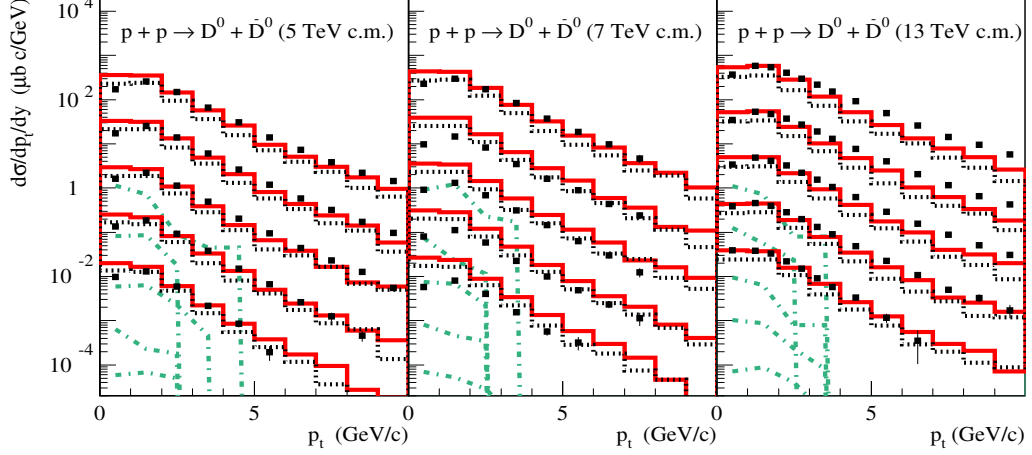


Figure 2: Transverse momentum dependence of $D^0 + \bar{D}^0$ production cross sections, for pp collisions at $\sqrt{s} = 5, 7$, and 13 TeV – left, middle, and right panels, respectively, for different rapidity intervals [from top to bottom: $2 < y < 2.5$ ($\times 10^0$), $2.5 < y < 3$ ($\times 10^{-1}$), $3 < y < 3.5$ ($\times 10^{-2}$), $3.5 < y < 4$ ($\times 10^{-3}$), $4 < y < 4.5$ ($\times 10^{-4}$)]. Solid histograms correspond to calculations using the default model parameters, with the partial contributions of IC being plotted as green dash-dotted lines, while dotted histograms are obtained using $\mu_F^c = \mu_R^c = 1.2m_{c,\perp}$ and $K_f^c = 2$ in the pQCD treatment. LHCb data [4, 5, 6] are shown by points.

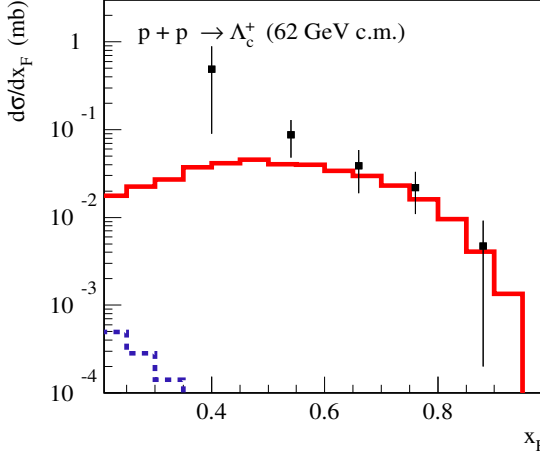


Figure 3: Calculated Feynman x dependence of the production cross section for Λ_c^+ , for pp collisions at $\sqrt{s} = 62$ GeV, and the partial contribution of the perturbative charm production – red solid and blue dashed histograms, respectively, compared to ISR data [19] (points).

5 Relevance to calculations of the prompt atmospheric neutrino flux

Regarding the relevance of charmed hadron production to calculations of the atmospheric neu-

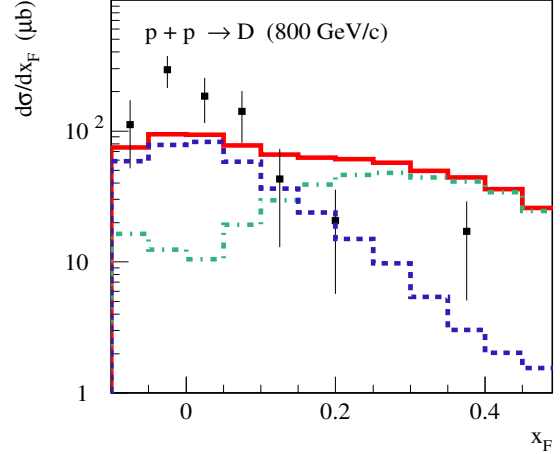


Figure 4: Calculated Feynman x dependence of the production cross section for D mesons, for pp collisions at 800 GeV/c, and partial contributions of the perturbative and nonperturbative production mechanisms – red solid, blue dashed, and green dash-dotted histograms, respectively, compared to the data of the LEBC-MPS collaboration [49] (points).

trino background, of importance is not the total $c\bar{c}$ pair production cross section plotted in Fig. 1 but rather the yield of charmed hadrons at

large values of Feynman x , $x_F \gtrsim 0.1$, which is a consequence of the steeply falling down primary CR spectrum. In particular, in the energy range where the primary proton flux can be approximated by a power law,

$$I_p(E_0) \simeq I_p(E_{\text{ref}}) (E_0/E_{\text{ref}})^{-\gamma_p}, \quad (8)$$

with E_{ref} being some reference energy and γ_p – the spectral slope, the proton contribution to the prompt neutrino background is proportional to spectrum-weighted moment of the distribution of charm (anti)quarks produced in proton-air collisions [43], the latter being defined as

$$Z_{p\text{-air}}^c(E, \gamma_p) = \int dx x^{\gamma_p-1} \frac{dn_{p\text{-air}}^c(E/x, x)}{dx}. \quad (9)$$

Here $dn_{p\text{-air}}^c/dx$ is the $c + \bar{c}$ distribution, with respect to the energy fraction $x = E/E_0$ taken from the parent proton.

The energy dependence of the perturbative contribution to $Z_{p\text{-air}}^c(E, \gamma_p)$, $Z_{p\text{-air}}^{c(\text{pert})}(E, \gamma_p)$, for $\gamma_p = 3$, calculated both for the default model settings and with $\mu_F^c = \mu_R^c = 1.2m_{c,\perp}$, $K_f^c = 2$, is plotted in Fig. 5. For comparison, the cor-

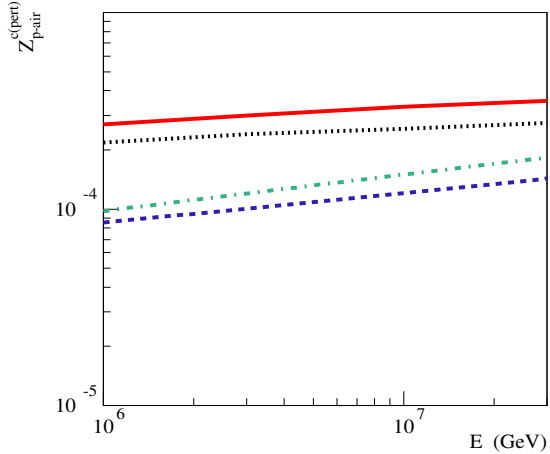


Figure 5: Energy dependence of $Z_{p\text{-air}}^{c(\text{pert})}$, for $\gamma_p = 3$, calculated with the default model settings or using $\mu_F^c = \mu_R^c = 1.2m_{c,\perp}$, $K_f^c = 2$ – red solid and black dotted lines, respectively. The results of NLO calculations based on gluon PDFs from CT14nlo_NF3 [50] and NNPDF31_nlo_pch_as_0118_nf_3 [51] PDF sets are plotted by, correspondingly, blue dashed and green dash-dotted lines.

responding results of NLO pQCD calculations

using different gluon PDFs, described in some detail in [43], for $\mu_F^c = \mu_R^c = m_{c,\perp}$, are shown. The differences between the presented results for $Z_{p\text{-air}}^{c(\text{pert})}$ are of the same order as the theoretical uncertainties of NLO calculations, estimated by varying the factorization and renormalization scales (see, e.g., Fig. 6 in [43]), and may give one some feeling about the uncertainties of the predictions for the prompt atmospheric neutrino flux, related to the perturbative treatment of charm production.

While our full scale calculation of the atmospheric neutrino background will be presented elsewhere, here we can provide rough estimations for the prompt contribution to the atmospheric muon neutrino (plus antineutrino) flux, $I_{\nu_\mu}(\text{prompt})$, both well below the energy of the so-called “knee” of the primary CR spectrum, $E_{\text{knee}} \simeq 3 - 4$ PeV [52], and above the “knee”, i.e., in the energy intervals where the relevant primary CR spectra can be approximated by a power law behavior.

Starting with the power law proton flux, Eq. (8), and proceeding like in [43] but factoring out only charmed hadron decay moments, we get for the primary proton contribution to $I_{\nu_\mu}(\text{prompt})$:

$$I_{\nu_\mu}^{(p)}(\text{prompt})(E) \simeq I_p(E_{\text{knee}}) \frac{(E/E_{\text{knee}})^{-\gamma_p}}{1 - Z_{p\text{-air}}^N(E, \gamma_p)} \times \sum_{h_c} Z_{p\text{-air}}^{h_c}(E, \gamma_p) Z_{h_c \rightarrow \nu_\mu}^{\text{dec}}(\gamma_p), \quad (10)$$

where we use $E_{\text{ref}} = E_{\text{knee}}$ and $Z_{p\text{-air}}^N$ is the spectrum-weighted moment for nucleon “regeneration”:

$$Z_{p\text{-air}}^N(E, \gamma_p) = \int dx x^{\gamma_p-1} \frac{dn_{p\text{-air}}^N(E/x, x)}{dx}, \quad (11)$$

with $dn_{p\text{-air}}^N/dx$ being the distribution of secondary nucleons in proton-air collisions.

In turn, $Z_{p\text{-air}}^{h_c}$ is the spectrum-weighted moment for charmed hadron h_c production in proton-air collisions while $Z_{h_c \rightarrow \nu_\mu}^{\text{dec}}$ is the moment for h_c decay into ν_μ :

$$Z_{p\text{-air}}^{h_c}(E, \gamma_p) = \int dx x^{\gamma_p-1} \frac{dn_{p\text{-air}}^{h_c}(E/x, x)}{dx} \quad (12)$$

$$Z_{h_c \rightarrow \nu_\mu}^{\text{dec}}(\gamma_p) = \int dx x^{\gamma_p-1} f_{h_c \rightarrow \nu_\mu}^{\text{dec}}(x). \quad (13)$$

Here $f_{h_c \rightarrow \nu_\mu}^{\text{dec}}(x)$ is the distribution for the energy fraction of h_c , taken by the neutrino, multiplied by the corresponding branching ratio.

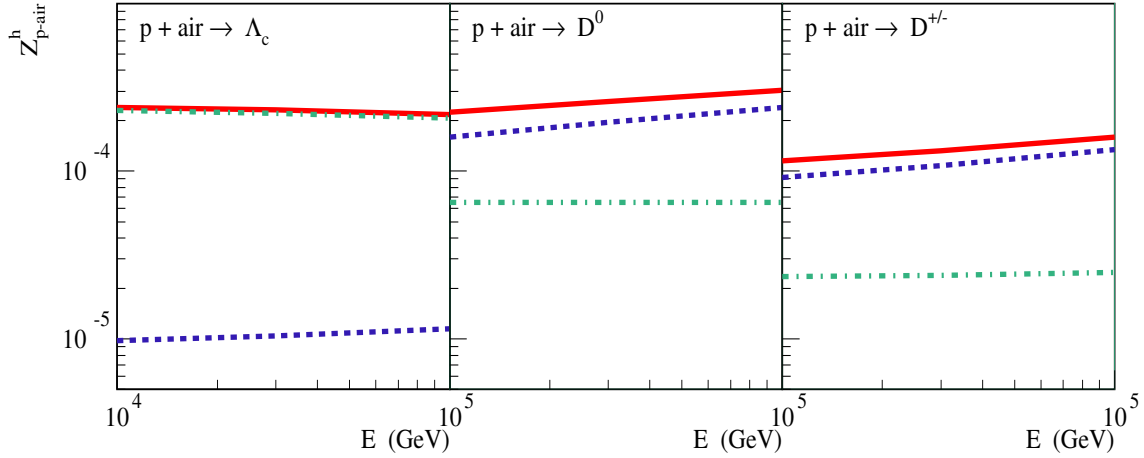


Figure 6: Calculated energy dependence of $Z_{p\text{-air}}^{h_c}$, for $\gamma_p = 2.7$, for $h_c = \Lambda_c + \bar{\Lambda}_c$ (left panel), $h_c = D^0 + \bar{D}^0$ (middle panel), and $h_c = D^\pm$ (right panel) – red solid lines. Partial contributions of the perturbative and nonperturbative mechanisms are plotted as blue dashed and green dash-dotted lines, respectively.

It is noteworthy that Eq. (10) is applicable both for the perturbative and IC contributions to the neutrino flux since we have not factorized out the fragmentation functions of charmed (anti)quarks into hadrons. This is quite important because we consider different hadronization mechanisms in the two cases.

In Fig. 6, we plot, for $\gamma_p = 2.7$, the energy dependence of the moments $Z_{p\text{-air}}^{h_c}$, between 10 and 100 TeV, for $h_c = \Lambda_c (+\bar{\Lambda}_c)$, $D^0 (+\bar{D}^0)$, and D^\pm , showing also the partial contributions of the perturbative and nonperturbative mechanisms. The same energy dependence at higher energies, between 1 and 10 PeV, is plotted in Fig. 7, for $\gamma_p = 3.2$. The two considered values of γ_p are characteristic for the slopes of the primary CR proton spectra below and above the “knee”, respectively [53, 54, 55, 56, 57]. While the perturbative mechanism provides the dominant contribution to the calculated moments for D meson production, for the chosen model parameters, an important correction, $\sim 20 - 30\%$, depending on the energy, comes from the IC content of the proton. On the other hand, regarding Λ_c production, the corresponding moment $Z_{p\text{-air}}^{\Lambda_c}$ is almost entirely defined by intrinsic charm, with the perturbative mechanism contributing less than 10%. In contrast to $\sigma_{pp}^{c\bar{c}}$ plotted in Fig. 1, where intrinsic charm provides a minor correction at the high energies of interest, its relative contribution to the CR spectrum-

weighted moments, Eq. (12), is enhanced due to the much harder energy spectra of secondary charmed hadrons, compared to the ones stemming from the perturbative mechanism. Further, as noticed previously in [43], we have a pretty flat energy dependence for the IC contributions to these CR spectrum-weighted moments, while observing a pronounced energy rise of the moments corresponding to the perturbative generation of charm, driven by the low x increase of the gluon PDF of the proton.

Regarding the contributions of primary CR nuclei, those can be well described using the so-called superposition model, reducing the problem to calculations of the CR spectrum-weighted moments $Z_{p\text{-air}}^{h_c}(E, \gamma_A)$ and $Z_{h_c \rightarrow \nu_\mu}^{\text{dec}}(\gamma_A)$, using the corresponding slopes γ_A for a primary nuclear mass group of interest (see, e.g., [43]). Thus, approximating the corresponding partial primary fluxes by a power law behavior, either below or above the respective spectral breaks $E_{\text{knee}}^{(A_i)}$,

$$I_{A_i}(E_0) \simeq I_{A_i}(E_{\text{knee}}^{(A_i)}) (E_0/E_{\text{knee}}^{(A_i)})^{-\gamma_{A_i}}, \quad (14)$$

γ_{A_i} being the corresponding spectral slopes, for the total prompt contribution to the atmospheric muon neutrino flux, we have [43]

$$I_{\nu_\mu}(\text{prompt})(E) \simeq \sum_i \frac{A_i^{2-\gamma_{A_i}} I_{A_i}(E_{\text{knee}}^{(A_i)})}{1 - Z_{p\text{-air}}^N(E, \gamma_{A_i})}$$

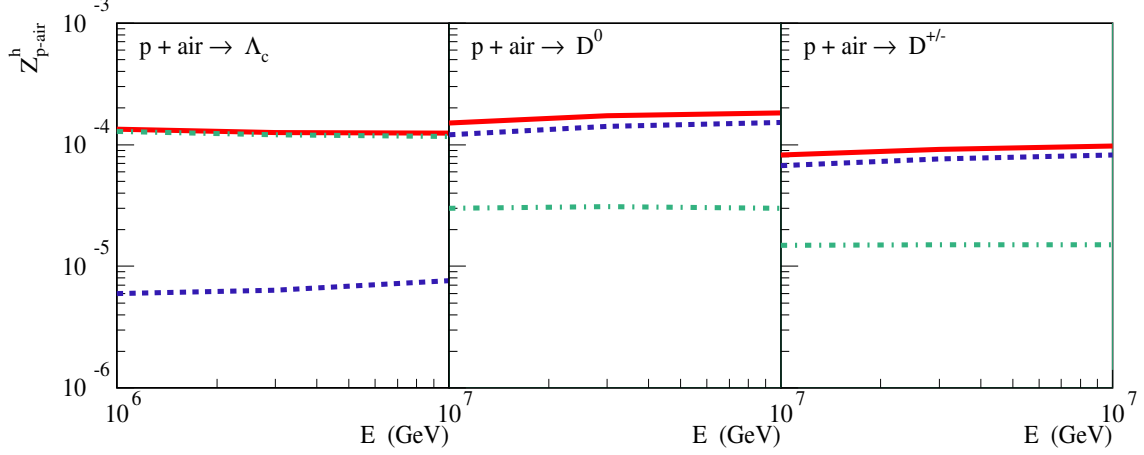


Figure 7: Same as in Fig. 6, for $\gamma_p = 3.2$.

$$\times \left[\frac{E}{E_{\text{knee}}^{(A_i)}} \right]^{-\gamma_{A_i}} \sum_{h_c} Z_{p\text{-air}}^{h_c}(E, \gamma_{A_i}) Z_{h_c \rightarrow \nu_\mu}^{\text{dec}}(\gamma_{A_i}). \quad (15)$$

In practice, contributions of primary nuclei heavier than helium can be neglected at 10% accuracy level.

Based on the data of the KASCADE-Grande [55] and Ice-Cube [57] experiments, we parametrize the primary fluxes of protons and helium above the corresponding “knees” as (see Fig. 8):

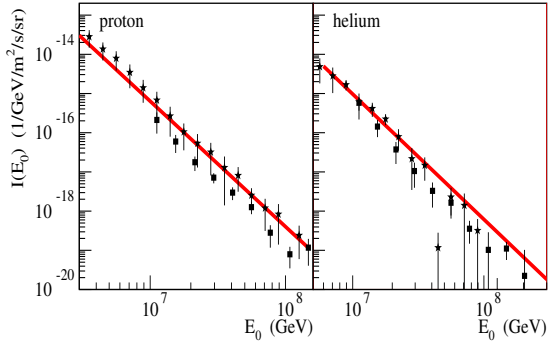


Figure 8: Parametrizations of the primary fluxes of protons (left) and helium (right) – red solid lines, compared to experimental data of KASCADE-Grande [55] (squares) and Ice-Cube [57] (stars).

$$\begin{aligned} I_p(E_0) &= I_p(E_{\text{knee}}^p) (E_0/E_{\text{knee}}^p)^{-3.2} \\ &\quad \times \Theta(E_0 - E_{\text{knee}}^p) \\ I_{\text{He}}(E_0) &= I_p(E_{\text{knee}}^{\text{He}}) (E_0/E_{\text{knee}}^{\text{He}})^{-3.2} \end{aligned} \quad (16)$$

$$\times \Theta(E_0 - E_{\text{knee}}^{\text{He}}), \quad (17)$$

with $E_{\text{knee}}^p = 3 \text{ PeV}$, $E_{\text{knee}}^{\text{He}} = 2E_{\text{knee}}^p$, $I_p(E_{\text{knee}}^p) = 3 \times 10^{-14} \text{ GeV}^{-1} \text{m}^{-2} \text{s}^{-1} \text{sr}^{-1}$, and $E_{\text{knee}}^{\text{He}} = 5 \times 10^{-15} \text{ GeV}^{-1} \text{m}^{-2} \text{s}^{-1} \text{sr}^{-1}$. Below the “knees”, we extend these primary spectra, using the slope equal -2.7 , which agrees with KASCADE data [53, 55], within the uncertainties of the experimental analysis.

Now, making use of Eq. (15) separately below and above the CR spectral breaks, inserting the nucleon regeneration moments $Z_{p\text{-air}}^N$ calculated with the QGSJET-III model and shown in Fig. 9, and using charmed hadron decay

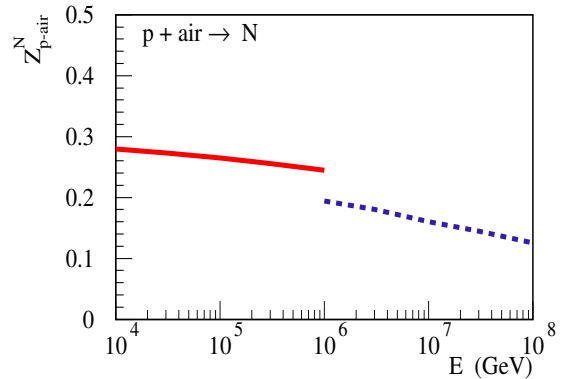


Figure 9: Calculated energy dependence of the nucleon regeneration moment $Z_{p\text{-air}}^N$, for $\gamma_p = 2.7$ (solid line) and $\gamma_p = 3.2$ (dashed line).

moments $Z_{h_c \rightarrow \nu_\mu}^{\text{dec}}$ complied in [58], we obtain prompt muon neutrino flux in the 10–100 TeV and 1–10 PeV energy intervals, plotted in Fig.

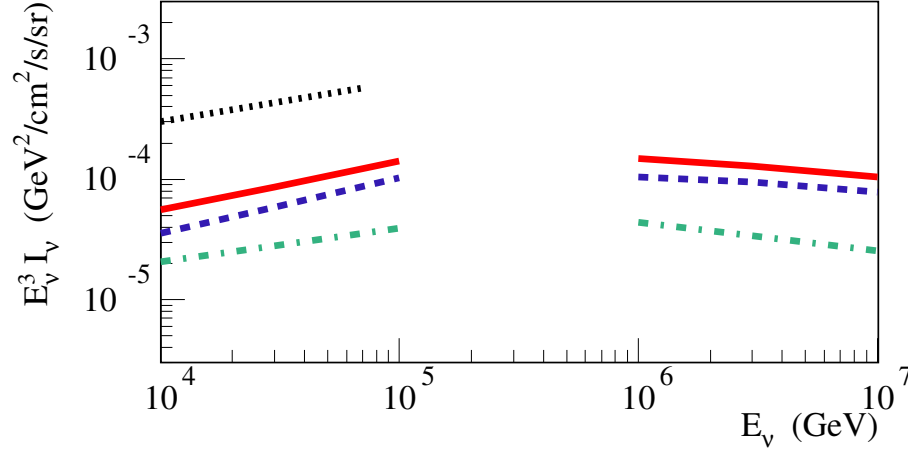


Figure 10: Calculated prompt atmospheric muon neutrino flux in the 10–100 TeV and 1–10 PeV energy intervals (red solid lines); partial contributions of the perturbative and nonperturbative charm production are plotted as blue dashed and green dash-dotted lines, respectively. The IceCube upper limit on the prompt atmospheric ν_μ background [20] is shown by black dotted line.

10, with the partial contributions of the perturbative charm production and of the intrinsic charm being shown as well. While the perturbative charm production dominates the prompt ν_μ flux both at low and high energies, the neutrino yield from intrinsic charm is also very significant, for the chosen model parameters, amounting to $\sim 25 - 35\%$ of the total flux, depending on the energy range.

We can also compare the calculated muon neutrino flux to the IceCube upper limit on the prompt ν_μ background [20], shown in Fig. 10 by the dotted line. As one can see in the Figure, the total predicted prompt muon neutrino flux is substantially below this limit. However, with a further increase of the statistics of the measurements and a refinement of the corresponding analysis methods (see, e.g., [59]), a direct detection of the prompt atmospheric neutrino flux looks quite feasible. Another point to keep in mind is the potential of IceCube to constrain the IC content of the proton, envisaged in [60]. With the contribution to the atmospheric neutrino fluxes from the perturbative charm production, being seriously constrained by LHCb data, even the current IceCube upper limit on the prompt ν_μ background does not leave too much space for the IC part, while much tighter constraints may be expected in the future.

A natural question concerns the uncertainties regarding our results for the prompt atmospheric

neutrino background. While this can not be answered quantitatively without a dedicated analysis which goes beyond the scope of the current work, we can discuss here the main sources of such uncertainties.

Generally predictions both for the conventional and for the prompt atmospheric neutrino backgrounds depend substantially on the parametrizations of the primary cosmic ray fluxes, employed in the corresponding calculations. This is not surprising since such parametrizations typically relied at very high energies ($E > 1$ PeV) on experimental results for the total cosmic ray flux, supplementing those by some plausible assumptions regarding the composition and the nature of potential sources of high energy cosmic rays. Consequently, the corresponding predictions for the primary proton flux at such high energies appeared to be rather uncertain and varied considerably from one parametrization to another. Since primary protons make $\sim 70\%$ of the prompt atmospheric neutrino background [cf. Eq. (15)], we preferred to rely on the data of the KASCADE-Grande [55] and Ice-Cube [57] experiments, regarding the fluxes of CR protons and helium. Yet the recently reported rather precise measurement of the primary proton flux by the LHAASO experiment [61] should provide a much more solid basis for calculations of the atmospheric neutrino background and reduce thereby considerably the

dependence of the results on the parametrizations of CR fluxes.

Coming now to the impact of uncertainties regarding the description of charmed hadron production, the least constrained remains the non-perturbative intrinsic charm contribution. As discussed in Section 4, our normalization for the IC content of the proton likely corresponds to the upper bound. How much smaller this normalization should be depends on a model treatment of the hadronization process, notably, on the strength of the “color drag” effect [62] in the corresponding string fragmentation procedures. The perturbative mechanism typically produces charm (anti)quarks at small (absolute) values of the rapidity in the c.m. frame, hence, at relatively small x . However, when such (anti)quarks are connected by strings (tubes) of color field to valence partons of the incident proton, the color force may “drag” them towards higher x . Therefore, if the mechanism is strong enough, the relevant experimental data on charm production at fixed target energies can be more or less described by the perturbative mechanism alone, thereby leaving little room for the IC contribution. Naively, one could have expected that the total, perturbative plus nonperturbative, charm production changes little in such a case. This is, however, not true because of the different energy dependence of the two contributions (cf. Fig. 1). Consequently, a model characterized by a stronger “color drag” effect would predict a higher prompt neutrino background (see, e.g., the corresponding discussion in [48]). Added to these are uncertainties regarding the large x behaviour of the gluon PDF of the proton. While this PDF is now substantially constrained in the low x limit by the LHCb measurements [4, 5, 6], the large x behaviour which impacts strongly the results (cf. Fig. 3 in [43]) remains much less constrained. Taking all this into account, the uncertainty of our calculation of the prompt atmospheric neutrino background may amount up to a factor of a few.

6 Discussion and conclusions

We presented a description of charm production in hadronic collisions, in the framework of the QGSJET-III MC generator, taking into consideration both the perturbative generation of

charm and the nonperturbative intrinsic charm contribution. The former is treated using the LO pQCD formalism, with the magnitude of the contribution being controlled by a K -factor, K_f^c , whose value has been fixed based on a comparison with LHCb data on D meson production. For IC, we employ a Regge-based formalism and, considering a Good-Walker expansion of hadron wave functions, assume that IC content of a particular GW Fock state is inverse proportional to the transverse size squared of that state. The relative importance of intrinsic charm is governed by a parameter specifying the IC content of the largest GW state considered of the proton, whose value has been fixed based on a comparison with experimental data on Λ_c baryon and D meson production at large values of Feynman x .

The extremely low IC content of the proton, smaller than one per mille, obtained by us, may seem surprising, in particular, in view of previous theoretical studies involving both an analysis of proton structure functions (SFs) (e.g., [14, 15]) or based on comparisons with charmed hadron production data (e.g., [63, 64]), which typically yielded an order of magnitude higher values. Regarding a SF analysis, the main support for a significant IC content of the proton comes from EMC studies of muon interactions in an iron target [65, 66, 67]. However, there was a serious caveat in the corresponding interpretations, revealed in [68]. To resolve very compact IC states, the virtual photon “probe” has to be pointlike enough, i.e., to be characterized by a sufficiently high virtuality, $q^2 \gtrsim 150 \text{ GeV}^2$, steeply rising with an increase of Bjorken x , which exceeds the values corresponding to the EMC measurements, in the kinematic range covered by the experiment [68]. Similar concerns apply to theoretical studies of Refs. [63, 64], where one considered a direct hard scattering of IC (anti)quark off a gluon or sea quark coming from the partner proton (nucleus): one allowed the momentum transfer squared for such a scattering to be as low as few GeV^2 , which gave rise to an “explosion” of the corresponding cross section in the small p_\perp limit. Taking properly into account the above-mentioned kinematic condition for resolving the intrinsic charm, the momentum transfer for such a hard scattering should be quite high, thereby making the direct scattering contribution negligibly small.

In contrast, we followed the approach of Ref. [41, 42], assuming that a scattering of *any* parton constituent of incident hadron is sufficient to destroy the coherence of the initial parton configuration of (a Fock state of) the hadron and thereby “to free the intrinsic charm from its virtual state” [42]. In such a case, the contribution of IC to charmed hadron production is approximately proportional to the total inelastic cross section for a reaction.

Regarding the importance of charmed hadron production for calculations of atmospheric neutrino background, the corresponding perturbative contribution can be conveniently studied at the level of CR spectrum-weighted moments for $c(\bar{c})$ production [43]. Comparing the energy dependence of these moments between our LO treatment and NLO calculations, the obtained differences appeared to be comparable to theoretical uncertainties of the latter, obtained by varying the factorization and renormalization scales.

However, for combining both the perturbative and nonperturbative contributions, one can only factorize out the decay moments for charmed hadrons, hence, to deal with production moments of those various hadrons: because the hadronization of IC (anti)quarks generally proceeds differently than for perturbatively generated ones. Comparing the energy-dependence of such moments, we observed, as expected, a rather flat one for the IC contribution, while having a pronounced energy-rise of the moments corresponding to perturbative generation of charm, driven by the low x increase of the gluon PDF of the proton. Consequently, as noticed earlier in [43], the perturbative contribution to the prompt atmospheric neutrino flux is characterized by a steeper energy-rise than the nonperturbative one.

To conclude, we developed a MC treatment of charmed hadron production, comprising the corresponding perturbative and nonperturbative mechanisms. Since the magnitude of the two contributions is controlled by independent adjustable parameters, one can use this fact for studying the uncertainties of the corresponding predictions and for further retuning the model, based on new experimental data both from accelerators and from astrophysical observatories.

Acknowledgments

The authors acknowledge useful discussions with M. V. Garzelli and other participants of the 2025 MIAPbP program “Event Generators at Colliders and Beyond Colliders”. S.O. acknowledges financial support from the Deutsche Forschungsgemeinschaft (projects 465275045 and 550225003). G.S. acknowledges support by the Bundesministerium für Bildung und Forschung, under grants 05A20GU2 and 05A23GU3, and by the Deutsche Forschungsgemeinschaft under Germany’s Excellence Strategy – EXC 2121 “Quantum Universe” – 390833306.

References

- [1] T. K. Gaisser, F. Halzen, and T. Stanev, *Particle astrophysics with high-energy neutrinos*, Phys. Rep. **258**, 173 (1995).
- [2] P. Nason, S. Dawson, and R. K. Ellis, *The one particle inclusive differential cross section for heavy quark production in hadronic collisions*, Nucl. Phys. B **327**, 49 (1989).
- [3] W. Beenakker, W. L. van Neerven, R. Meng, G. A. Schuler, and J. Smith, *QCD corrections to heavy quark production in hadron hadron collisions*, Nucl. Phys. B **351**, 507 (1991).
- [4] R. Aaij et al. (LHCb Collaboration), *Prompt charm production in pp collisions at $\sqrt{s} = 7$ TeV*, Nucl. Phys. B **871**, 1 (2013).
- [5] R. Aaij et al. (LHCb Collaboration), *Measurements of prompt charm production cross-sections in pp collisions at $\sqrt{s} = 13$ TeV*, JHEP **03**, 159 (2016).
- [6] R. Aaij et al. (LHCb Collaboration), *Measurements of prompt charm production cross-sections in pp collisions at $\sqrt{s} = 5$ TeV*, JHEP **06**, 147 (2017).
- [7] R. Gauld, J. Rojo, L. Rottoli, and J. Talbert, *Charm production in the forward region: constraints on the small- x gluon and backgrounds for neutrino astronomy*, JHEP **11**, 009 (2015).

- [8] O. Zenaiev et al. (PROSA Collaboration), *Impact of heavy-flavour production cross sections measured by the LHCb experiment on parton distribution functions at low x*, Eur. Phys. J. C **75**, 396 (2015).
- [9] R. Gauld and J. Rojo, *Precision determination of the small- x gluon from charm production at LHCb*, Phys. Rev. Lett. **118**, 072001 (2017).
- [10] O. Zenaiev, M. V. Garzelli, K. Lipka, S.-O. Moch, A. Cooper-Sarkar, F. Olness, A. Geiser, and G. Sigl (PROSA Collaboration), *Improved constraints on parton distributions using LHCb, ALICE and HERA heavy-flavour measurements and implications for the predictions for prompt atmospheric-neutrino fluxes*, JHEP **04**, 118 (2020).
- [11] R. E. Nelson, R. Vogt, and A. D. Frawley, *Narrowing the uncertainty on the total charm cross section and its effect on the J/ψ cross section*, Phys. Rev. C **87**, 014908 (2013).
- [12] S. J. Brodsky, P. Hoyer, C. Peterson, and N. Sakai, *The intrinsic charm of the proton*, Phys. Lett. B **93**, 451 (1980).
- [13] S. J. Brodsky, C. Peterson, and N. Sakai, *Intrinsic heavy-quark states*, Phys. Rev. D **23**, 2745 (1981).
- [14] T. J. Hobbs, J. T. Londergan, and W. Melnitchouk, *Phenomenology of nonperturbative charm in the nucleon*, Phys. Rev. D **89**, 074008 (2014).
- [15] P. Jimenez-Delgado, T. J. Hobbs, J. T. Londergan, and W. Melnitchouk, *New limits on intrinsic charm in the nucleon from global analysis of parton distributions*, Phys. Rev. Lett. **114**, 082002 (2015).
- [16] V. A. Bednyakov, S. J. Brodsky, A. V. Lipatov, G. I. Lykasov, M. A. Malyshev, J. Smiesko, and S. Tokar, *Constraints on the intrinsic charm content of the proton from recent ATLAS data*, Eur. Phys. J. C **79**, 92 (2019).
- [17] S. Ostapchenko, *QGSJET-III model of high energy hadronic interactions: The formalism*, Phys. Rev. D **109**, 034002 (2024).
- [18] S. Ostapchenko, *QGSJET-III model of high energy hadronic interactions: II. Particle production and extensive air shower characteristics*, Phys. Rev. D **109**, 094019 (2024).
- [19] G. Bari et al., *A Measurement of Λ_c^+ baryon production in proton proton interactions at $\sqrt{s} = 62$ GeV*, Nuovo Cim. A **104**, 571 (1991).
- [20] M. G. Aartsen et al. (IceCube Collaboration), *Observation and characterization of a cosmic muon neutrino flux from the northern hemisphere using six years of IceCube data*, Astrophys. J. **833**, 3 (2016).
- [21] V. N. Gribov, *A reggeon diagram technique*, Sov. Phys. JETP **26**, 414 (1968).
- [22] V. N. Gribov, *Glauber corrections and the interaction between high-energy hadrons and nuclei*, Sov. Phys. JETP **29**, 483, (1969).
- [23] V. N. Gribov and L. N. Lipatov, *Deep inelastic $e p$ scattering in perturbation theory*, Sov. J. Nucl. Phys. **15**, 438 (1972).
- [24] G. Altarelli and G. Parisi, *Asymptotic freedom in parton language*, Nucl. Phys. B **126**, 298 (1977).
- [25] Yu. L. Dokshitzer, *Calculation of the structure functions for deep inelastic scattering and $e^+ e^-$ annihilation by perturbation theory in quantum chromodynamics*, Sov. Phys. JETP **46**, 641 (1977).
- [26] H. J. Drescher, M. Hladik, S. Ostapchenko, and K. Werner, *A Unified treatment of high-energy interactions*, J. Phys. G **25**, L91 (1999).
- [27] H. J. Drescher, M. Hladik, S. Ostapchenko, T. Pierog, and K. Werner, *Parton based Gribov-Regge theory*, Phys. Rep. **350**, 93 (2001).
- [28] S. Ostapchenko, H. J. Drescher, F. M. Liu, T. Pierog, and K. Werner, *Consistent treatment of soft and hard processes in hadronic interactions*, J. Phys. G **28**, 2597 (2002).
- [29] S. Ostapchenko, *On the re-summation of enhanced Pomeron diagrams*, Phys. Lett. B **636**, 40 (2006).

- [30] S. Ostapchenko, *Enhanced Pomeron diagrams: Re-summation of unitarity cuts*, Phys. Rev. D **77**, 034009 (2008).
- [31] S. Ostapchenko, *Total and diffractive cross sections in enhanced Pomeron scheme*, Phys. Rev. D **81**, 114028 (2010).
- [32] V. A. Abramovsky, V. N. Gribov, and O. V. Kancheli, *Character of inclusive spectra and fluctuations produced in inelastic processes by multi-pomeron exchange*, Sov. J. Nucl. Phys. **18**, 308 (1974).
- [33] S. Ostapchenko, *Monte Carlo treatment of hadronic interactions in enhanced Pomeron scheme: QGSJET-II model*, Phys. Rev. D **83**, 014018 (2011).
- [34] J. C. Collins, D. E. Soper, and G. F. Sterman, *Factorization of hard processes in QCD*, Adv. Ser. Direct. High Energy Phys. **5**, 1 (1989).
- [35] S. Ostapchenko, *Nonlinear screening effects in high energy hadronic interactions*, Phys. Rev. D **74**, 014026 (2006).
- [36] S. Ostapchenko and M. Bleicher, *Double parton scattering: impact of nonperturbative parton correlations*, Phys. Rev. D **93**, 034015 (2016).
- [37] R. K. Ellis, W. J. Stirling and B. R. Webber, *QCD and collider physics*, Camb. Monogr. Part. Phys. Nucl. Phys. Cosmol. **78** (1996), 1, Cambridge University Press, 2011.
- [38] A. B. Kaidalov, *J/ψ $c\bar{c}$ production in e^+e^- and hadronic interactions*, JETP Lett. **77**, 349 (2003).
- [39] A. B. Kaidalov and O. I. Piskunova, *Inclusive spectra of baryons in the Quark-Gluon String model*, Z. Phys. C **30**, 145 (1986).
- [40] A. B. Kaidalov, *Quark and diquark fragmentation functions in the model of quark gluon strings*, Sov. J. Nucl. Phys. **45**, 902 (1987).
- [41] S. J. Brodsky and P. Hoyer, *Nucleus as a color filter in QCD: Hadron production in nuclei*, Phys. Rev. Lett. **63**, 1566 (1989).
- [42] S. J. Brodsky, P. Hoyer, A. H. Mueller, and W.-K. Tang, *New QCD production mechanisms for hard processes at large x* , Nucl. Phys. B **369**, 519 (1992).
- [43] S. Ostapchenko, M. V. Garzelli, and G. Sigl, *On the prompt contribution to the atmospheric neutrino flux*, Phys. Rev. D **107**, 023014 (2023).
- [44] M. L. Good and W. D. Walker, *Diffractive dissociation of beam particles*, Phys. Rev. **120**, 1857 (1960).
- [45] L. Frankfurt, M. Strikman, D. Treleani, and C. Weiss, *Evidence for color fluctuations in the nucleon in high-energy scattering*, Phys. Rev. Lett. **101**, 202003 (2008).
- [46] P. Chauvat et al. (R608 Collaboration), *Production of Λ_c with large x_F at the ISR*, Phys. Lett. B **199**, 304 (1987).
- [47] F. G. Garcia et al. (SELEX Collaboration), *Hadronic production of Λ_c from 600 GeV/c π^- , Σ^- and p beams*, Phys. Lett. **B528**, 49 (2002).
- [48] A. Bhattacharya, R. Enberg, M. H. Reno, I. Sarcevic, and A. Stasto, *Prompt atmospheric neutrino fluxes: perturbative QCD models and nuclear effects*, JHEP **11**, 167 (2016).
- [49] R. Ammar et al. (LEBC-MPS Collaboration) *D-Meson production in 800-GeV/c pp interactions*, Phys. Rev. Lett. **61**, 2185 (1988).
- [50] S. Dulat, T.-J. Hou, J. Gao, M. Guzzi, J. Huston, P. Nadolsky, J. Pumplin, C. Schmidt, D. Stump, and C.-P. Yuan, *New parton distribution functions from a global analysis of quantum chromodynamics*, Phys. Rev. D **93**, 033006 (2016).
- [51] R. D. Ball et al. (NNPDF Collaboration), *Parton distributions from high-precision collider data*, Eur. Phys. J. C **77** (2017) 663.
- [52] G. Kulikov and G. Khristiansen, *On the size spectrum of extensive air showers*, Sov. Phys. JETP **8**, 441 (1959).

- [53] T. Antoni et al. (KASCADE Collaboration), *KASCADE measurements of energy spectra for elemental groups of cosmic rays: Results and open problems*, *Astropart. Phys.* **24**, 1 (2005).
- [54] W. D. Apel et al. (KASCADE-Grande Collaboration), *Knee-like structure in the spectrum of the heavy component of cosmic rays observed with KASCADE-Grande*, *Phys. Rev. Lett.* **107**, 171104 (2011).
- [55] W. D. Apel et al. (KASCADE-Grande Collaboration), *KASCADE-Grande measurements of energy spectra for elemental groups of cosmic rays*, *Astropart. Phys.* **47**, 54 (2013).
- [56] W. D. Apel et al. (KASCADE-Grande Collaboration), *Ankle-like feature in the energy spectrum of light elements of cosmic rays observed with KASCADE-Grande*, *Phys. Rev. D* **87**, 081101 (2013).
- [57] M. G. Aartsen et al. (IceCube Collaboration), *Cosmic ray spectrum and composition from PeV to EeV using 3 years of data from IceTop and IceCube*, *Phys. Rev. D* **100**, 082002 (2019).
- [58] M. Thunman, G. Ingelman, and P. Gondolo, *Charm production and high energy atmospheric muon and neutrino fluxes*, *Astropart. Phys.* **5**, 309 (1996).
- [59] J. Boettcher et al. (IceCube Collaboration), *Search for the Prompt Atmospheric Neutrino Flux in IceCube*, *PoS ICRC2023*, 1068 (2023) [arXiv:2309.07560 [astro-ph.HE]].
- [60] R. Laha and S. J. Brodsky, *IceCube can constrain the intrinsic charm of the proton*, *Phys. Rev. D* **96**, 123002 (2017).
- [61] Z. Cao et al. (LHAASO Collaboration), *First Identification and Precise Spectral Measurement of the Proton Component in the Cosmic-Ray ‘Knee’*, [arXiv:2505.14447 [astro-ph.HE]].
- [62] E. Norrbin and T. Sjostrand, *Production and hadronization of heavy quarks*, *Eur. Phys. J. C* **17**, 137 (2000).
- [63] A. V. Giannini, V. P. Goncalves, and F. S. Navarra, *Intrinsic charm contribution to the prompt atmospheric neutrino flux*, *Phys. Rev. D* **98**, 014012 (2018).
- [64] R. Maciula and A. Szczurek, *Intrinsic charm in the nucleon and charm production at large rapidities in collinear, hybrid and k_T -factorization approaches*, *JHEP* **10**, 135 (2020).
- [65] J. J. Aubert et al. (EMC Collaboration), *A study of dimuon events in 280 GeV muon interactions*, *Phys. Lett. B* **94**, 96 (1980).
- [66] J. J. Aubert et al. (EMC Collaboration), *An experimental limit on the intrinsic charm component of the nucleon*, *Phys. Lett. B* **110**, 73 (1982).
- [67] J. J. Aubert et al. (EMC Collaboration), *Production of charmed particles in 250 GeV μ^+ -iron interactions*, *Nucl. Phys. B* **213**, 31 (1983).
- [68] J. Blümlein, *A Kinematic condition on intrinsic charm*, *Phys. Lett. B* **753**, 619 (2016).